

Spectral transitions of an ultraluminous X-ray source, NGC 2403 Source 3

Naoki ISOBE ¹, Kazuo MAKISHIMA ^{1,2}, Hiromitsu TAKAHASHI ³, Tsunefumi MIZUNO ³,
Ryouhei MIYAWAKI ², Poshak GANDHI ¹, Madoka KAWAHARADA ¹, Atsushi SENDA ¹,
Tessei YOSHIDA ^{4,5}, Aya KUBOTA ⁶, Hiroshi KOBORI ⁶,

¹*Cosmic Radiation Laboratory, the Institute of Physical and Chemical Research,
2-1 Hirosawa, Wako, Saitama, 351-0198, Japan*

isobe@crab.riken.jp

²*Department of Physics, University of Tokyo, 7-3-1 Hongo, Bunkyo-ku, Tokyo, Japan*

³*Department of Physics, Hiroshima University,*

1-3-1 Kagamiyama, Higashi-Hiroshima, Hiroshima 739-8526, Japan

⁴*Institute of Space and Astronautical Science, Japan Aerospace Exploration Agency (ISAS/JAXA),
3-1-1 Yoshinodai, Sagami-hara-shi, Kanagawa 229-8510, Japan*

⁵*Department of Physics, Tokyo University of Science,*

1-3 Kagurazaka, Shinjuku-ku, Tokyo 162-8601, Japan

⁶*Department of Electronic Information Systems, Shibaura Institute of Technology,
307 Fukasakum Minuma-ku, Saitama-shi, Saitama, 337-8570, Japan*

(Received 0 0; accepted 0 0)

Abstract

Suzaku observation of an ultraluminous X-ray source, NGC 2403 Source 3, performed on 2006 March 16–17, is reported. The Suzaku XIS spectrum of Source 3 was described with a multi-color black-body-like emission from an optically thick accretion disk. The innermost temperature and radius of the accretion disk was measured to be $T_{\text{in}} = 1.08_{-0.03}^{+0.02}$ keV and $R_{\text{in}} = 122.1_{-6.8}^{+7.7} \alpha^{1/2}$ km, respectively, where $\alpha = (\cos 60^\circ / \cos i)$ with i being the disk inclination. The bolometric luminosity of the source was estimated to be $L_{\text{bol}} = 1.82 \times 10^{39} \alpha$ ergs s⁻¹. Archival Chandra and XMM-Newton data of the source were analyzed for long-term spectral variations. In almost all observations, the source showed multi-color black-body-like X-ray spectra with parameters similar to those in the Suzaku observation. In only one Chandra observation, however, Source 3 was found to exhibit a power-law-like spectrum, with a photon index of $\Gamma = 2.37 \pm 0.08$, when it was fainter by about $\sim 15\%$ than in the Suzaku observation. The spectral behavior is naturally explained in terms of a transition between the slim disk state and the “very high” states, both found in Galactic black hole binaries when their luminosity approach the Eddington limit. These results are utilized to

argue that ultraluminous X-ray sources generally have significantly higher black-hole masses than ordinary stellar-mass black holes.

1. Introduction

Since the era of the Einstein observatory (Fabbiano & Trinchieri 1987), luminous point-like X-ray sources, of which X-ray luminosities exceed a few times 10^{39} ergs s^{-1} , were frequently found at off-center regions of nearby normal galaxies. These X-ray sources are called ultraluminous X-ray Sources (ULXs; Makishima et al. 2000). The nature of ULXs has remained one of the important unresolved issues in X-ray astrophysics, for nearly three decades.

Both observational (e.g., Mizuno et al. 2001; Kubota & Makishima 2004; Tsunoda et al. 2006; Mizuno et al. 2007; Isobe et al. 2008) and theoretical (e.g., Watarai et al. 2000) studies suggest that the X-ray properties of ULXs resemble those of Galactic black hole binaries (BHBs) in high accretion rates. However, we currently have two distinct interpretations of ULXs; intermediate mass BHBs with a mass of $M \gg 10M_{\odot}$ (where M_{\odot} is the solar mass) radiating at sub- or trans-Eddington luminosities, and stellar-mass BHBs shining at highly super-Eddington luminosities. We urgently need to distinguish the two alternative.

X-ray spectra of well-studied ULXs are approximated by either a multi-color disk (MCD; Mitsuda et al. 1984; Makishima et al. 1986) model or a power-law (PL) one (or their combination). Furthermore, several ULXs are reported to show a spectral transition between the MCD-like and PL-like states (e.g., Kubota et al. 2001). These properties could be explained, in the simplest manner, by regarding the MCD-like and PL-like states as analogous to the classical high/soft and low/hard states of Galactic BHBs, respectively. However, this naive interpretation has encountered several difficulties (e.g., Makishima et al. 2000; Mizuno et al. 2001; Kubota et al. 2002).

Recent observational studies (e.g, Tsunoda et al. 2006) revealed that the X-ray spectra of the MCD-like ULX requires a temperature profile in the accretion disk that is flatter than those in the standard accretion disk (Shakura & Sunyaev 1973) assumed in the MCD model. The flat temperature profile is theoretically predicted by a concept of slim accretion disk (Watarai et al. 2000), in which an optically-thick advection and/or photon trapping (e.g., Ohsuga et al. 2005) become important due to high accretion rates. The slim disk interpretation can solve several basic problems with the MCD model, including too-high disk temperatures and variable innermost disk radii (Mizuno et al. 2001; Watarai et al. 2000) . Therefore, the MCD-like ULX is thought to harbor a slim accretion disk rather than a standard disk. On the other hand, photon indices of the PL-like ULXs ($\Gamma > 2.0$; e.g., Kubota et al. 2002) are steeper than those of the classical low/hard state BHBs ($\Gamma = 1.5 - 2.0$; e.g, Tanaka 1997). Because such a steep photon index is observed from Galactic BHBs when they are in the very high state (VHS; Miyamoto et al. 1991) in which Comptonization plays an important role (Kubota & Makishima 2004),

the PL-like ULXs are thought to be in the VHS (Kubota et al. 2002). In the recent Suzaku (Mitsuda et al. 2007) observation of a nearby normal galaxy NGC 1313, Mizuno et al. (2007) have reinforced the VHS and slim disk state interpretations of two ULXs therein, X1 and X2, respectively.

So far, these typical ULX properties have been observed from objects with very high luminosities (e.g., $\gtrsim 10^{40}$ ergs s $^{-1}$), which require either a high BH mass or an extreme super-Eddington condition (or both). If, however, such ULX properties are confirmed in less luminous objects with a luminosity within a few times the Eddington limit of Galactic stellar-mass BHBs, we will become sure that the ULX phenomena can appear without highly-supper Eddington luminosities. Particularly important is to search for spectral transitions among such objects.

Source 3 (hereafter, Src 3) in the nearby spiral (SABcd) galaxy NGC 2403 is one of the most suitable targets for our purpose. Originally discovered by the Einstein observatory (Fabbiano & Trinchieri 1987), it was later revealed with ASCA to exhibit an MCD-type spectrum with an innermost disk temperature of $T_{\text{in}} = 1.10_{-0.09}^{+0.10}$ keV and an innermost disk radius of $R_{\text{in}} = 130$ km (Kotoku et al. 2000). Furthermore, its bolometric luminosity, $L_{\text{bol}} \sim 2 \times 10^{39}$ ergs s $^{-1}$, places it in between luminous ULX and ordinary stellar-mass BHBs. In order to examine whether this object exhibits the ULX-like behavior, we conducted a Suzaku observation of NGC 2403; then the object was again found in the MCD-like state. We also utilized Chandra and XMM-Newton archival data of Src 3, and discovered a spectral transition that resembles those observed in more luminous ULXs. In the present paper, these results are utilized to strengthen the classification of Src 3 as a ULX with a rather modest luminosity. We employ the distance to NGC 2403 of 3.2 ± 0.4 Mpc (Freedman & Madore 1998), as determined from observations of Cepheid variables.

2. Suzaku Observation and Data Reduction

The Suzaku observation of NGC 2403 was conducted on 2006 March 16–17, during the science working group phase. The X-ray Imaging spectrometer (XIS; Koyama et al. 2007) and the Hard X-ray Detector (HXD; Takahashi et al. 2007; Kokubun et al. 2007) onboard Suzaku were operated in the normal clocking mode without any window option, and in the normal mode, respectively. The nucleus of the NGC 2403 galaxy was placed at the XIS nominal position (Serlemitsos et al. 2007).

Utilizing the HEADAS 6.5.1 software package, we reprocessed the data from the Revision 2 processing, and created new cleaned event files. The present paper concentrates on the XIS data, because no significant X-ray signals were detected with the HXD in this observation. We screened the data under the following criteria; the spacecraft is outside the south Atlantic anomaly (SAA), the time after an exit from the SAA is larger than 436 s, the geometric cut-off rigidity is higher than 6 GV, the source elevation above the rim of bright and night Earth is higher than 20° and 5°, respectively, and the XIS data are free from telemetry saturation. As

a result, we have obtained 62.7 ks of good exposure. In the scientific analysis below, we utilize only those events with a grade of 0, 2, 3, 4, or 6.

3. Results

3.1. X-ray Image

Figure 1 shows a 0.5 – 10 keV Suzaku XIS image of NGC 2403, superposed on an optical image taken from the Digitized Sky Survey (DSS; Lasker et al. 1990). Two bright point-like X-ray sources are clearly seen in the figure; the brighter and fainter of them correspond to Src 3 and Source 5 (hereafter Src 5; Fabbiano & Trinchieri 1987), respectively.

In addition to the point sources, we clearly observe faint X-ray emission, extending along the optical galaxy. The detailed properties of this extended (possibly diffuse) X-ray emission will be reported in a separate paper (Senda et al. 2008). In the summer of 2004, a supernova, SN2004dj, exploded in this galaxy (Nakano et al. 2004). Although X-ray emission from SN2004dj was detected with Chandra in 2004 (Pooley & Lewin 2004) at a 0.5 – 8 keV flux of 1.2×10^{-13} ergs s⁻¹ cm⁻², we found no significant X-ray enhancement at the location of the supernova (the filled star in figure 1) above a 0.5 – 8 keV flux upper limit of 1×10^{-14} ergs s⁻¹ cm⁻².

3.2. X-ray spectrum of NGC 2403 Src 3

We integrated X-ray signals of Src 3 within a circle denoted as **Src3** in figure 1. The background spectrum was derived within a circle **BGD3**. In order to reduce possible contributions from the extended X-ray emission, we adopted a radius of 2' (corresponding to 1.86 kpc at the distance of 3.2 Mpc) for these regions, which is slightly smaller than a typical integration region used in the Suzaku analysis of point sources ($\sim 3'$).

Figure 2 shows background-subtracted two-band X-ray lightcurves of Src 3, obtained with the three front-illuminated (FI) CCD cameras (XIS 0, 2 and 3; Koyama et al. 2007) of the XIS. Summed over the three FI CCDs, the time-averaged count rate of Src 3 is measured to be 0.112 ± 0.002 cts s⁻¹ and 0.078 ± 0.002 cts s⁻¹ in the soft (0.5 – 2 keV) and hard (2 – 10 keV) bands, respectively. The data suggest a variation on a time-scale of $\gtrsim 10$ ks in the middle of the observation, it is statistically insignificant ($\chi^2/\text{d.o.f.} = 10.2/14$ and $11.2/14$ for the soft and hard band, respectively). As a result, the hardness is found to be rather constant throughout the exposure. Below, we hence analyze the time-averaged spectrum of Src 3.

Figure 3 shows background-subtracted XIS spectra of NGC 2403 Src 3, presented without removing the instrumental response. The X-ray spectra obtained with FI and background-illuminated (BI) CCD camera (XIS 1; Koyama et al. 2007) were both binned into energy intervals each with at least 100 events. Thus, the X-ray signals were significantly detected over the 0.4–10 keV range. The spectrum appears to be rather featureless, without any clear sign of emission or absorption features.

To analyze the spectra, we calculated a response matrix function (rmf) and an auxiliary response file (arf), using `xisrmfgen` and `xissimarfgen` (Ishisaki et al. 2007), respectively. The reduction of the effective area due to contaminants on the optical blocking filters of the XIS was taken into account by `xissimarfgen`. We performed the spectral fitting using XSPEC version 12.4.0.

We fitted the Src 3 spectra with the MCD and PL models, as a standard way in analyzing the spectra of Galactic BHBs and ULXs. The FI and BI spectra were jointly fitted, with the model normalization allowed to differ between them. We found that the fluxes from BI and FI spectra agreed with each other, within 4%.

Conducting the spectral fitting, we found the absorption column density, which was left free, to fall below the Galactic line-of-sight value of $N_{\text{H}} = 4.1 \times 10^{20} \text{ cm}^{-2}$ toward NGC 2403 (Dickey & Lockman 1990). This effect may be ascribed to residual soft diffuse emission within the Src 3 region, which remains even after subtracting signals from the BGD3 region, due to brightness gradients. According to Senda et al. (2008), the diffuse emission in NGC 2403 can be described by thermal plasma emission model with two temperatures of $\sim 0.26 \text{ keV}$ and $\sim 0.74 \text{ keV}$, having a metallicity of ~ 0.44 solar. We hence took into account the contamination, by adding two APEC components in XSPEC with the temperature fixed at $kT = 0.26 \text{ keV}$ and 0.74 keV , both of which were subjected to the Galactic absorption. Their relative normalization was fixed at the value determined with the total diffuse emission (Senda et al. 2008), while their summed luminosity was left free. We left free the absorption to the ULX component.

The spectral parameters obtained in this analysis are summarised in table 1. The PL model was rejected with $\chi^2 = 349.4/174$, because the observed X-ray spectrum has a more convex shape, as revealed by residuals in figure 3. On the other hand, the MCD model successfully described the X-ray spectrum of Src 3 with $\chi^2 = 182.0/174$. The derived absorption column density for the ULX component, $N_{\text{H}} = 1.40_{-0.42}^{+0.45} \times 10^{21} \text{ cm}^{-2}$, is higher by a factor of about 3 than the Galactic value, but this amount of excess absorption is attributed reasonably to that within the NGC 2403 galaxy, and/or an additional absorber localized around the source. The thermal plasma components were found to have only a negligible contribution to the observed spectrum, with a 0.5 – 10 keV luminosity of $L_{\text{th}} = 3.5 \times 10^{37} \text{ ergs s}^{-1}$. This luminosity is reasonable in view of the results by Senda et al. (2008).

The innermost disk temperature of Src 3 was obtained as $T_{\text{in}} = 1.08_{-0.03}^{+0.02} \text{ keV}$. The X-ray flux was measured to be $1.1 \times 10^{-12} \text{ ergs cm}^{-2} \text{ s}^{-1}$ in the 0.7 – 7 keV range, without correcting for absorption. These give an absorption-corrected bolometric luminosity of $L_{\text{bol}} = 1.82 \times 10^{39} \alpha \text{ ergs s}^{-1}$, with $\alpha = (\cos 60^\circ / \cos i)$ where i is the inclination of the accretion disk to our line of sight. The value of T_{in} agrees with that obtained with ASCA in 1997 (Kotoku et al. 2000) within statistical errors, while L_{bol} is lower by about 20%. Through a relation $L_{\text{bol}} = 4\pi\sigma r_{\text{in}}^2 T_{\text{in}}^4$, with σ being the Stefan-Boltzmann constant, the apparent innermost disk radius is calculated as $r_{\text{in}} = 102.6_{-5.8}^{+6.4} \text{ km}$. The true innermost radius is determined as $R_{\text{in}} = 122.1_{-6.8}^{+7.7} \alpha^{1/2} \text{ km}$, applying

the correction as $R_{\text{in}} = \xi \kappa^2 r_{\text{in}}$, where $\xi = 0.412$ is a correction factor for the inner boundary condition (Kubota et al. 1998), and $\kappa = 1.7$ is a spectral hardening factor (Shimura & Takahara 1995) which represents the ratio of the color temperature to the effective temperature.

We also examined the “variable- p ” disk model, in which the dependence of the local temperature on the radius r from the BH is assumed to scale as r^{-p} , with the index p being a positive free parameter (Mineshige et al. 1994). While this model with $p = 0.75$ reduces to a simple MCD model, that with smaller value of p , down to 0.5, is considered to approximate the X-ray spectra from a slim disk (Watarai et al. 2000; Kubota & Makishima 2004; Mizuno et al. 2001; Mizuno et al. 2007). The fit was acceptable, but with no significant improvement ($\chi^2 = 181.9/173$) over the MCD fit. All the parameters became consistent with those of the MCD model; $p = 0.73_{-0.07}^{+0.12}$, $T_{\text{in}} = 1.09 \pm 0.07$ keV, and $R_{\text{in}} = 116.4_{-28.7}^{+39.4}$ km.

4. Analysis of Chandra and XMM-Newton Data

In order to better understand the nature of Src 3, its intensity-correlated spectral variations are considered to be of particular importance (e.g, Mizuno et al. 2001). Therefore, we analyzed the archival Chandra and XMM-Newton data of NGC 2403.

4.1. Chandra observations

So far, 5 Chandra ACIS exposures toward NGC 2403 have been conducted, 4 of which were motivated by the discovery of SN2004dj (Nakano et al. 2004). However, NGC 2403 Src 3 was within the ACIS field of view on only three occasions. Furthermore, in the first observation performed on 2001 April 17 (ObsID = 2014), the ACIS spectrum of NGC 2403 Src 3 was severely distorted by event pileup ($\gtrsim 30\%$; Schlegel & Pannuti 2003). Therefore, we analyzed only the data in the remaining two observations (ObsID = 4628 and 4630), wherein Src 3 was placed at a relatively large distance from the ACIS aimpoint (see $\Delta\theta$ in table 2), so that a broadened point spread function made the event pileup insignificant. The log of these two observations is shown in table 2. The data were read out in the timed-exposure mode with the standard frame time of 3.2 s, and telemetered in the FAINT format. In ObsID = 4628 and 4630, Src 3 was placed on ACIS-S3 (a BI chip) and S2 (an FI one), respectively.

Utilizing the CIAO 3.4 software and referring to CALDB 3.3.0.1, we reprocessed all the data to create new level-2 event files in the standard manner. We removed `acis_detect_afterglow` correction, and applied a “new” bad pixel file created by `acis_run_hotpix`¹. After removing X-ray point sources detected by `wavdetect` within the ACIS field of view, we produced a 0.3 - 12 keV lightcurve covering the entire CCD chip, and then discarded those time intervals where the count rate exceeds 120% of that averaged during the observation. This procedure gave us the good exposures as listed in table 2. The ACIS spectra of NGC 2403 Src 3 were extracted within a circle centered on the X-ray peak, and

¹ http://asc.harvard.edu/ciao3.4/guides/acis_data.html

those of BGD from a concentric annulus. The radii of these regions are also shown in table 2. The `rmf` and `arf` files were generated, assuming an X-ray point source, with the CIAO tools `mkacisrmf` and `mkarf`, respectively.

4.2. XMM-Newton observations

So far, XMM-Newton observations of NGC 2403 have been performed 5 times. However, only the data obtained in three of them are public at present, of which the observational log is given in table 3. Although the results in the individual observations were separately reported by several authors (Feng & Kaaret 2005; Stobbart et al. 2006; Winter et al. 2006), we re-analyzed all the data in a systematic way. The third observation (ObsID = 0164560901) was motivated by the explosion of SN2004dj. On all these occasions, the EPIC MOS and pn cameras were operated in the nominal full frame mode. The medium optical-blocking filter was adopted in the first and second observations (ObsID = 0150651101 and 0150651201, respectively), while the thick one was utilized in the third observation. In the first and second observations, we do not use the pn data, because Src 3 fell on the gap of the pn chips.

We used the Science Analysis System (SAS) version 7.0.0 to reduce the XMM-Newton data. All data were reprocessed by `emchain` or `epchain`, based on the Current Calibration Files (CCF), which was latest at the beginning of our analysis (2007 July). After Read & Ponman (2003), we rejected high-background periods, using the point-source removed lightcurve with `PATTERN == 0` and `#XMMEA_EM/P` in 10 – 15 keV. As a result, we obtained good exposures, as shown in table 3. For the spectral analysis, MOS events with `PATTERN ≤ 12`, `#XMMEA_EM` and `FLAG = 0`, and pn ones with `PATTERN ≤ 4`, `#XMMEA_EP` and `FLAG = 0`, were finally selected.

We integrated the EPIC spectra of NGC 2403 Src 3 and BGD, within a circle of 36'' radius and an annulus of 72''–108'' radius, respectively, both centered on Src 3. Because the pn image of the third observation revealed a faint point-like source within the BGD annulus, a circle of 30'' radius around this contaminating source was removed from both MOS and pn data. We created the `rmf` and `arf`, utilizing the SAS tools, `rmfgen` and `arfgen` respectively.

4.3. Spectral modeling

Figure 4 compares the Chandra and XMM-Newton spectra of NGC 2403 Src 3 with the Suzaku one, in the form of the unfolded spectrum (panel a) and of the ratio to the Suzaku best-fit MCD model (panel b). All the data are presented in 0.7 – 7 keV, where the energy ranges of all the three instruments overlap. In the Chandra (4628) and XMM-Newton (0164560901) observations, the spectral shape of Src 3 thus coincides well with those in the Suzaku observation, indicating that the source was in the MCD-like spectral state on these occasions. In addition, the spectral normalization is similar, to within $\sim 20\%$, among these three data sets. In contrast, the X-ray spectrum in the Chandra observation of ObsID = 4630 exhibits a distinct and less convex shape, which is approximated by a power-law, at least above ~ 1 keV where the effect

of interstellar absorption become unimportant. The flux on this occasion is estimated to be lower by about 15% than that in the Suzaku observation. In figure 4, the deconvolved spectra have been derived using the absorbed MCD or PL model (whichever is more successful) to be described below.

The raw Chandra and XMM-Newton spectra of Src 3 in the individual observations are shown in figures 5 and 6, respectively. We applied the MCD and PL models to these spectra, in the same way as for the Suzaku data, and obtained the results summarised in table 4. We neglected the contamination from the diffuse X-ray emission associated with the host galaxy, because the integration area, we adopted for Chandra and XMM-Newton data, were more than an order of magnitude smaller than that for Suzaku data. As figure 4 suggests, the MCD model better reproduced the observed X-ray spectra in general, except for that from the Chandra observation of ObsID = 4630. When the source was in the MCD-like state, the spectral parameters exhibited only small deviations from the Suzaku measurements. The bolometric luminosity of Src 3 was found to vary only about 10% among these observations. Similar MCD parameters were reported by Feng & Kaaret (2005) and Stobbart et al. (2006), based on the third XMM-Newton observation.

The Chandra spectrum of ObsID = 4630, in contrast, was better reproduced by a PL model with a photon index of $\Gamma = 2.37 \pm 0.08$. The X-ray flux on this occasion, 9.3×10^{-13} ergs $\text{cm}^{-2} \text{s}^{-1}$ in the 0.7 – 7 keV range, was lowest among the data sets analyzed here. The absorption column density became larger by a factor of about 2 – 3 than those in the other observations; $N_{\text{H}} = 3.73_{-0.33}^{+0.35} \times 10^{21} \text{ cm}^{-2}$. Similarly, an apparent N_{H} change was reported from a transient ULX, CXOU J132518.2-430304, which was discovered within the host galaxy of Centaurus A (Sivakoff et al. 2008). However, such significant changes in N_{H} , associated with transitions between the PL-like and MCD-like states, are uncommon among Galactic BHBs. Therefore, this N_{H} change from Src 3 is likely to be an artifact, caused presumably because a simple PL model is inappropriate to describe the softest end of the Chandra spectrum from ObsID=4630. We discuss this issue briefly in section 5.

Although the MCD model gave a better fit than the PL model to all the XMM-Newton data, the third XMM-Newton dataset still exhibit some residuals with $\chi^2/\text{d.o.f.} = 637.9/568$ (figure 6c). This urged us to apply the variable- p disk model to this dataset and the other MCD-like ones, as we did for the Suzaku spectrum. Then, all the spectra in the MCD-like states were successfully reproduced by the variable- p disk model. The fit was significantly improved in the third XMM-Newton observation and the Chandra ObsID = 4628, and yielded $p = 0.58_{-0.02}^{+0.03}$ and $0.60_{-0.05}^{+0.07}$, respectively.

5. Discussion

In the Suzaku observation of NGC 2403 performed on 2006 March 16 – 17, Src 3 exhibited a curved 0.4 – 10 keV spectrum, which can be reproduced by the MCD model. We obtained

the innermost disk temperature and radius of the source as $T_{\text{in}} = 1.08_{-0.03}^{+0.02}$ keV and $R_{\text{in}} = 122.1_{-6.8}^{+7.7} \alpha^{1/2}$ km, respectively. The bolometric luminosity of the source was measured as $L_{\text{bol}} = 1.82 \times 10^{39} \alpha$ ergs s $^{-1}$. Making use of the archival Chandra and XMM-Newton data, we found the source to exhibit similar MCD-type spectrum on 4 occasions, while a PL-shaped spectrum on one occasion (Chandra observation of ObsID = 4630) when the 0.7 – 7 keV flux was about 15% and 17% lower than those in the Suzaku observation and the Chandra observation of ObsID = 4628, respectively. This flux change between the MCD-like and PL-like states are larger than the relative flux uncertainties between Suzaku, Chandra, and XMM-Newton ($\lesssim 10\%$; e.g., Reeves et al. 2007; Bamba et al. 2008; Ishida et al. 2008).

In the MCD-like states, T_{in} and L_{bol} of Src 3 exhibited only small variations across more than 8 years from the ASCA observation (Kotoku et al. 2000) to the Suzaku one. Both of these parameters are located at the lowest end of those of typical ULXs. The value of R_{in} derived in these observations corresponds to the radius of the last stable orbit, $3R_{\text{S}}$ (R_{s} being the Schwarzschild radius), around a non-rotating BH with a mass of $\sim 13\alpha^{1/2}M_{\odot}$. Because the Eddington luminosity of such a BH becomes $L_{\text{E}} \sim 2 \times 10^{39} \alpha^{1/2}$ ergs s $^{-1}$, the properties of Src 3 in the MCD-like states can be understood consistently as a $\sim 13M_{\odot}$ BH radiating at close to L_{E} , wherein a standard accretion disk is formed down to $\sim 3R_{\text{S}}$, like in the high/soft state of normal Galactic BHBs. This apparently reconfirms the conclusion by Kotoku et al. (2000). Then, can we really explain the overall behavior of Src 3, by assuming that it was in the standard high/soft state during the Suzaku observation ?

One difficulty with the high/soft state interpretation comes from the fact that the third XMM-Newton dataset preferred a variable- p disk model with $p = 0.58_{-0.02}^{+0.03}$, which is smaller than that in the standard accretion disk. To see this in a systematic manner, we plotted in figure 7, the parameters determined from the variable- p disk model, against the observed X-ray flux in the 0.7 – 7 keV range. Although errors are rather large, the plot reveals a tendency that R_{in} and p become smaller, and T_{in} gets higher, as the flux increases. Such behavior is numerically predicted by the slim disk model (e.g., Watarai et al. 2000; Ohsuga 2006). The correlation is not affected significantly by possible flux uncertainties among the three satellites, because the three XMM-Newton data points reveal the same behavior. Therefore, it is natural to regard that the source was actually in the slim disk state during these observations. Moreover, figure 7 indicates that Src 3 was in the transition regime between the standard high/soft state ($p = 0.75$) and the slim disk regime ($p \leq 0.75$) when observed with Suzaku.

Another difficulty with the high/soft interpretation is provided by the spectral transition, revealed by the Chandra data (ObsID = 4630), when the source was $\sim 15\%$ less luminous than in the Suzaku data. The spectral slope of this PL-like state, $\Gamma = 2.37 \pm 0.08$, is too steep for the source to be interpreted as in the low/hard state ($\Gamma = 1.5 - 2.0$; e.g, Tanaka 1997), which would be realized when the source becomes less luminous than in the high/soft state. In contrast, this steep slope agrees very well with those of Galactic BHBs in the VHS (Miyamoto

et al. 1991; Kubota & Done 2004). Furthermore, Galactic BHBs have been observed to become less luminous when they make a transition from the slim disk state to the VHS (Kubota & Makishima 2004; Abe et al. 2005). These comparisons suggest that the PL-like state of Src 3 corresponds to the VHS.

Since Comptonization of disk photons by hot coronae is thought to become important in the VHS (Kubota & Makishima 2004), we tried a Comptonization model, **compTT** in XSPEC (Titarchuk 1994), on the Chandra spectrum of Src 3 in ObsID = 4630. The electron temperature of the Comptonizing coronae was fixed at $T_e = 20$ keV, as seen in the VHS of XTE J1550-564 (Kubota & Done 2004). The model successfully described the data with parameters shown in table 5, giving a fit goodness similar to that with the PL model. The optical depth of the corona, $\tau = 1.2 \pm 0.1$, is comparable to those of the Galactic BHB in the VHS ($\tau \sim 2$; e.g., Kubota et al. 2001; Kubota & Done 2004). Furthermore, the value of N_H has become consistent with those found in the MCD-like states; this is because the Comptonized continuum flattens in energies below that of the seed photons ($T_{\text{seed}} \sim 0.25$ keV). Although the derived value of T_{seed} is lower than the disk temperature $T_{\text{in}} \sim 1.1$ keV measured in the MCD-like state, the discrepancy could be due to a disk truncation at a radius larger than that of the last stable orbit, as is suggested in the “strong” VHS of XTE J1550-564 (Kubota & Done 2004).

From these considerations, we conclude that NGC 2403 Src 3 normally resides at the lowest end of the slim disk state and makes occasional transitions into the VHS. Since the dominance of these two spectral states is regarded as an essential property of the ULXs (e.g., Kubota et al. 2002; Tsunoda et al. 2006; Mizuno et al. 2007), we may regard Src 3 as a ULX, in spite of its moderate luminosity. In addition, we may regard Src 3 as radiating at $\sim L_E$, for the following two reasons. One is that the transitions of BHBs between the VHS and the slim disk state is observed at $\gtrsim 0.3L_E$ (Kubota & Makishima 2004; Abe et al. 2005), while the other is that the value of $p \sim 0.75$ would not be observed if the source were radiating with $\gg L_E$. Thus, L_{bol} of the source gives the BH mass as $M \sim 10 - 20M_\odot$.

We may independently estimate the BH mass using R_{in} determined by the variable- p disk model. In this case, the simple assumption of $R_{\text{in}} = 3R_S$ would underestimate a mass of the BH that hosts a slim disk, because the X-ray photons would also be radiated from the region inside the last stable orbit (Watarai et al. 2000). Recently, Vierdayanti et al. (2008) evaluated a factor to correct the underestimation as 1.2 – 1.6, by analyzing numerically simulated X-ray spectra from the slim disk with the variable- p disk model (the extended disk black body model in their paper) for a wide range of mass accretion rate. Combining this correction factor and R_{in} derived from our variable- p disk model fit (figure 7b), we estimate the BH mass of NGC 2403 Src 3 as $M = 9 - 15M_\odot$. This value agrees very well with that derived from the Eddington limit argument. Therefore, we can consistently interpret the available data of NGC 2403 Src 3, by considering that it hosts a BH with a mass of $M = 10 - 15M_\odot$, radiating at $\sim L_E$.

Finally, let us discuss implications of the present results on the ULX phenomenon in

general. Obviously, they do not give direct support to the intermediate mass BH interpretation of ULX, since the observed luminosity of Src 3 is well within the Eddington limits of ordinary-mass stellar BH. Nevertheless, one important discovery is that this relatively low-luminosity object exhibits clear ULX behavior, including in particular a transition between the slim disk state and the VHS. In other words, the ULX phenomenon appears even at a luminosity range of $\sim 2 \times 10^{39}$ ergs s⁻¹. This is within ~ 3 times the Eddington luminosity of any stellar-mass BHs, even if we consider the least massive known BHBs as GRO J0422+32 ($3.97 \pm 0.95 M_{\odot}$; Gelino & Harrison 2003), GRO J1655-40 ($5.5-7.9 M_{\odot}$; Shahbaz et al. 1999), and GX 339-4 ($5.8 \pm 0.5 M_{\odot}$; Hynes et al. 2003). Consequently, the ULX behaviour in this case does not require any highly (~ 10) super-Eddington luminosity. Extrapolating this conclusion to more luminous ULXs, we suggest that they are not radiating at highly super-Eddington luminosities, either, even though their mass accretion rates are very likely to be "super-critical". That is, ULXs are thought to be BHs which are significantly more massive than Galactic BHBs, accreting matter at super-critical rates, and yet radiating at about their Eddington limit.

We are grateful to all the members of the Suzaku team, for the successful operation and calibration. We also thank Dr. Ohsuga for his valuable theoretical comments. This research has made use of the archival Chandra data and its related software provided by the Chandra X-ray Center (CXC). A part of the result is based on the observation obtained with XMM-Newton, an ESA science mission with instruments and contributions directly funded by ESA Member States and NASA. We have made extensive use of the NASA/IPAC Extra galactic Database (NED; the Jet Propulsion Laboratory, California Institute of Technology, the National Aeronautics and Space Administration). The optical DSS image of NGC 2403 was downloaded from SkyView ². The ROSAT source catalog were taken from the ROSAT Source Browser by Dr. Englhauser ³.

References

- Abe, Y., Fukazawa, Y., Kubota, A., Kasama, D., & Makishima, K., 2005, PASJ, 57, 629
 Bamba A., et al. 2008, in prep.
 Dickey, J. M., & Lockman, F. J. 1990, ARA&A, 28, 215
 Fabbiano, G., & Trinchieri, G., 1987, ApJ, 315, 46
 Feng, H., & Kaaret, P., 2005, ApJ, 633, 1052
 Freedman, W. L., & Madore, B. F., 1988, ApJ, 332, L63
 Gelino, D. M., & Harrison T. E., 2003, ApJ, 599, 1254
 Hynes, R. I., Steeghs, D., Casares, J., Charles P. A., & O'Brien, K., 2003, ApJ, 583, L95

² <http://skyview.gsfc.nasa.gov/>

³ <http://www.xray.mpe.mpg.de/cgi-bin/rosat/src-browser>

Ishida M., et al. 2008 in prep.

Isobe, N., Kubota, A., Makishima, K., Gandhi, P., Griffiths, R.E., Dewangan, G.C., Itho, T., & Mizuno, T., 2008, PASJ, 60S, 241

Ishisaki, Y., et al. 2007, PASJ, 59, 113

Kokubun, M., et al., 2007, PASJ, 59, S53

Kotoku, J., Mizuno, T., Kubota, A., & Makishima, K., 2000, PASJ, 52, 1081

Koyama K., et al., 2007, PASJ, 59, S23

Kubota, A., Done, C., & Makishima, K. 2002, MNRAS, 337, L11

Kubota, A., & Done, C., 2004 MNRAS, 353, 980

Kubota, A., Makishima, K., & Ebisawa, K., 2001, ApJ, 560, L147

Kubota, A., & Makishika, K., 2004, ApJ, 601, 428

Kubota, A., Mizuno, T., Makishima, K., Fukazawa, Y., Kotoku, J., Ohnishi, T., & Tashiro, M., 2001, ApJ, 547, L119

Kubota, A., Tanaka, Y., Makishima, K., Ueda, Y., Dotani, T., Inoue, H., & Yamaoka, Y. 1998, PASJ, 50, 667

Lasker, B. M., Sturch, C. R., McLean, B. J.; Russell, J. L., Jenkner, H.; Shara, M. M., AJ, 99, 2019

Makishima, K., Maejima, Y., Mitsuda, K., Bradt, H. V., Remillard, R. A., Tuohy, I. R., Hoshi, R., Nakagawa, M., 1986, ApJ, 308, 635

Makishima, K., et al., 2000, ApJ, 535, 632

Mineshige, S., Hirano, A., Kitamoto, S., Tamada, T. T., Fukue, J. 1994, ApJ, 426, 308

Mitsuda, K., et al., 1984, PASJ, 36, 741

Mitsuda, K., et al., 2007, PASJ, 59, S1

Miyamoto, S., Kimura, K., Kitamoto, S., Dotani, T., & Ebisawa, K., 1991, ApJ, 383, 784

Mizuno, T., Kubota, A., & Makishima, K., 2001, ApJ, 554, 1282

Mizuno, T., et al., 2007, PASJ, 59, S257

Nakano, S., Itagaki, K., Bouma, R. J., Lehky, M., & Hornoch, K. 2004, IAU Circ., 8377

Ohsuga, K., 2006, ApJ, 640, 923

Ohsuga, K., Mori, M., Nakamoto, T., & Mineshige, S. 2005, ApJ, 628, 368

Pooley, D., & Lewin, W. H. G., 2004, IAU Circ., 8390, 1

Read, A. M., & Ponman, T. J., 2003, A&A, 409, 395

Reeves, J. N., et al., 2007, PASJ, 59, S301

Schlegel, E. M., & Pannuti, T. G., 2003, AJ, 125, 3025

Serlemitsos, P.J, et al., 2007, PASJ, 59, S9

Senda, A., et al., 2008, in prep.

Shahbaz, T., van der Hooft, F., Casares, J., Charles, P. A., & van Paradijs, J., 1999, MNRAS, 306, 89

Shakura N. I., & Sunyaev, R. A. 1973, A&A, 24, 337

Shimura, T., & Takahara, F. 1995, ApJ, 445, 780

Sivakoff, G. R., et al. 2008, ApJ, 677, L27

Stobart, A. -M., Roberts, T. P., & Wilms, J., 2006, MNRAS, 368, 397

Takahashi, T., et al., 2007, PASJ, 59, S35

- Tanaka, Y., 1997, in *Accretion Disks – New Aspects*, Proceedings of the EARA Workshop Held in Garching, Germany, (Lecture Notes in Phys., 487; Springer Berlin / Heidelberg)
- Titarchuk, L., 1994, *ApJ*, 434, 570
- Tsunoda, N., Kubota, A., Namiki, M., Sugiho, M., Kawabata, K., & Kazuo, M. 2006, *PASJ*, 58, 1081
- Vierdayanti, K., Watarai, K., & Mineshige, S., 2008, *PASJ*, 60, 653
- Watarai, K., Fukue, J., & Mineshige, S. 2000, *PASJ*, 52, 133
- Winter, L. M., Mushotzky, R. F., & Reynolds, C .S., 2006, *ApJ*, 649, 730

Table 1. Best-fit parameters to the Suzaku spectra of Src 3.

Model	MCD	variable- p	PL
N_{H} (10^{21} cm $^{-2}$)	$1.40^{+0.45}_{-0.42}$	$1.52^{+1.02}_{-0.74}$	$8.66^{+0.69}_{-0.65}$
T_{in} (keV)	$1.08^{+0.02}_{-0.03}$	1.09 ± 0.07	–
p, Γ *	–	$0.73^{+0.12}_{-0.07}$	2.79 ± 0.07
R_{in} (km)	$122.1^{+7.7}_{-6.8}$	$116.4^{+39.4}_{-28.7}$	–
L †	1.82	1.89	4.10
L_{th} ‡	0.035	0.038	0.174
$\chi^2/\text{d.o.f.}$	182.0/174	181.9/173	349.4/174

* Index p of radial temperature dependence for the variable- p model, or the photon index Γ for the PL one.

† L_{bol} for the MCD and variable- p model, or absorption-corrected 0.5 – 10 keV luminosity for the PL model, both in 10^{39} ergs s $^{-1}$.

‡ Absorption-corrected 0.5 – 10 keV luminosity of the sum of the two APEC components, in 10^{39} ergs s $^{-1}$.

Table 2. Log of archival Chandra observations of NGC 2403, utilized in the present paper.

ObsID	4628	4630
Date	2004 Aug 23	2004 Dec 22
Exposure (ks)	46.5	48.7
Mode	Timed Exposure	
Frame Time	3.2 s	
Format	FAINT	
ACIS Chip*	S3	S2
$\Delta\theta$ †	5'.8	4'.9
r_{Src3} ‡	15''.7	13''.8
r_{BGD} §	19''.6–23''.6	17''.7–21''.6
Signal (cts s $^{-1}$)	0.16	0.11

* ACIS CCD chip on which Src 3 is located.

† Off axis angle of Src 3 from the aim point

‡ Radius of the source integration circle.

§ Radius of the BGD integration annulus.

|| Count rate of Src 3 in 0.3 – 10 keV

Table 3. Log of archival XMM-Newton observations of NGC 2403.

ObsID		0150651101	0150651201	0164560901
Date		2003 Apr 30	2003 Sep 11	2004 Sep 12–13
Mode		Full Frame		
Filter		Thin	Thin	Medium
Exposure (ks)	MOS1	5.26	6.98	57.1
	MOS2	5.52	7.20	56.2
	pn	–	–	49.6

Table 4. Summary of fitting to the Chandra and XMM-Newton spectra of Src 3

Instrument	ObsID	Model	N_{H} (10^{21} cm^{-2})	T_{in} (keV)	p, Γ *	R_{in} (km)	L †	$\chi^2/\text{d.o.f.}$
Chandra	4628	MCD	$1.47^{+0.15}_{-0.14}$	1.06 ± 0.04	–	$127.4^{+8.8}_{-8.3}$	1.86	166.9/156
		variable- p	2.23 ± 0.44	$1.23^{+0.15}_{-0.11}$	$0.60^{+0.07}_{-0.05}$	$70.3^{+28.1}_{-20.8}$	2.48	158.4/155
		PL	$3.83^{+0.26}_{-0.24}$	–	$2.28^{+0.07}_{-0.06}$	–	2.62	230.0/156
	4630	MCD	$0.97^{+0.21}_{-0.19}$	$1.04^{+0.05}_{-0.04}$	–	$115.3^{+11.0}_{-9.9}$	1.42	194.8/123
		variable- p	$3.55^{+0.34}_{-0.32}$	$3.3(> 2.3)$	0.46 ± 0.01	$4.19^{+6.64}_{-3.87}$	10.4	109.9/122
		PL	$3.73^{+0.35}_{-0.33}$	–	2.37 ± 0.08	–	2.14	110.7/123
XMM-Newton	0150651101	MCD	$1.40^{+0.43}_{-0.38}$	1.09 ± 0.10	–	$116.5^{+23.0}_{-19.2}$	1.72	31.1/37
		variable- p	$1.44^{+1.31}_{-0.96}$	$1.10^{+0.34}_{-0.18}$	$0.74^{+1.81}_{-0.18}$	$112.4^{+81.9}_{-68.8}$	1.75	31.1/36
		PL	$3.77^{+0.76}_{-0.66}$	–	$2.23^{+0.18}_{-0.17}$	–	2.42	46.3/37
	0150651201	MCD	$1.66^{+0.41}_{-0.36}$	1.11 ± 0.09	–	$116.5^{+20.8}_{-17.6}$	1.87	33.7/45
		variable- p	$2.14^{+1.15}_{-1.22}$	$1.21^{+0.38}_{-0.23}$	$0.65^{+0.40}_{-0.11}$	$83.1^{+110.4}_{-48.5}$	2.16	33.2/44
		PL	$4.15^{+0.71}_{-0.64}$	–	$2.22^{+0.16}_{-0.15}$	–	2.65	47.5/45
	0164560901	MCD	1.66 ± 0.07	1.06 ± 0.02	–	$130.9^{+4.8}_{-4.6}$	1.95	637.9/568
		variable- p	$2.59^{+0.22}_{-0.21}$	1.27 ± 0.06	$0.58^{+0.03}_{-0.02}$	$64.3^{+11.1}_{-10.1}$	2.85	585.6/567
		PL	$4.30^{+0.13}_{-0.12}$	–	2.43 ± 0.03	–	2.81	943.3/568

* Index p of radial temperature dependence for the variable- p model, or the photon index Γ for the PL model.† L_{bol} for the MCD and variable- p model, or absorption-corrected 0.5 – 10 keV luminosity for the PL model, both in $10^{39} \text{ ergs s}^{-1}$.

Table 5. Parameters of compTT fitting to the Chandra spectrum of ObsID = 4630.

Parameters	Value
N_{H} (10^{21} cm $^{-2}$)	$1.4^{+2.6}_{-0.7}$
T_{seed}^* (keV)	0.25(< 0.29)
T_{e}^\dagger (keV)	20 (fix)
τ^\ddagger	1.15 ± 0.11
$\chi^2/\text{d.o.f.}$	111.14/122

* Energy of seed soft photons

† Electron temperature of the Comptonizing corona

‡ Optical depth of the Comptonizing corona

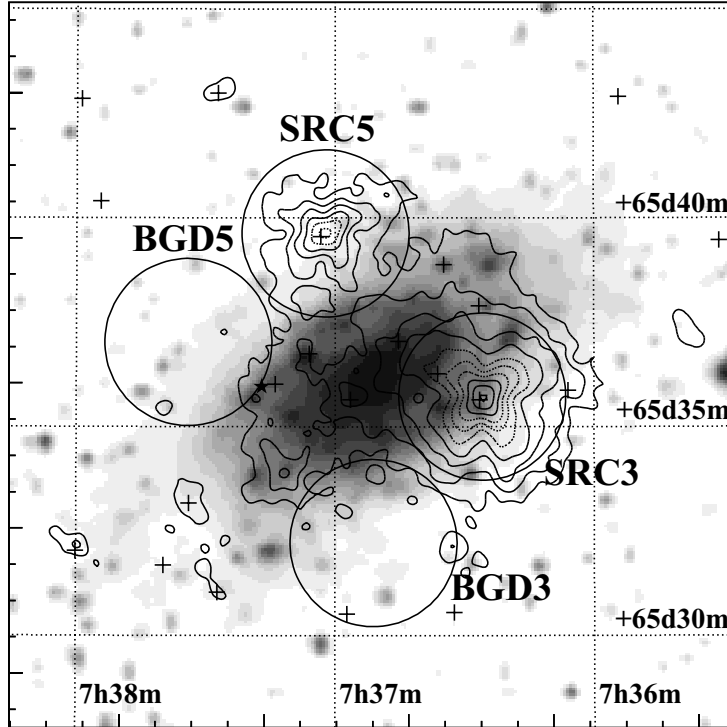


Fig. 1. Suzaku XIS contour image of NGC 2403 in the 0.5 – 10 keV range, overlaid on the optical DSS gray-scale image. Data from all the XIS CCD chip are summed up. Neither background-subtraction nor exposure-correction is performed to the image. The source signals of Src 3 and the associated background are integrated within **Src3** and **BGD3**, while those of Src 5 are extracted from **Src5** and **BGD5**. The positions of the ROSAT X-ray sources, taken from the second ROSAT source catalog of pointed observations with the position sensitive proportional counter (2RXP), are indicated with crosses, and that of SN2004dj with the filled star.

BGD-subtracted Lightcurve of NGC 2403 Src3

XIS FI

Bin time: 5760. s

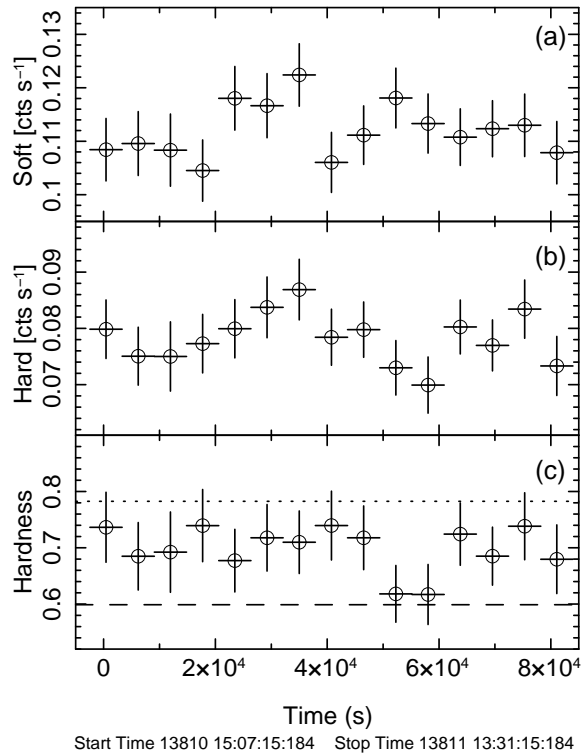


Fig. 2. Background-subtracted XIS FI lightcurve of NGC 2403 Src 3. Each time bin is set to 5760 s, corresponding to the orbital period of Suzaku. Panels (a) and (b) show the soft (0.5 – 2 keV) and hard (2 – 10 keV) energy band lightcurves, respectively. The hardness, simply calculated as the ratio of the hard band count rate to the soft band one, is shown in panel (c). Dashed and dotted lines in panel (c) indicate predictions by MCD models with of $T_{\text{in}} = 1.0$ keV and 1.2 keV, respectively.

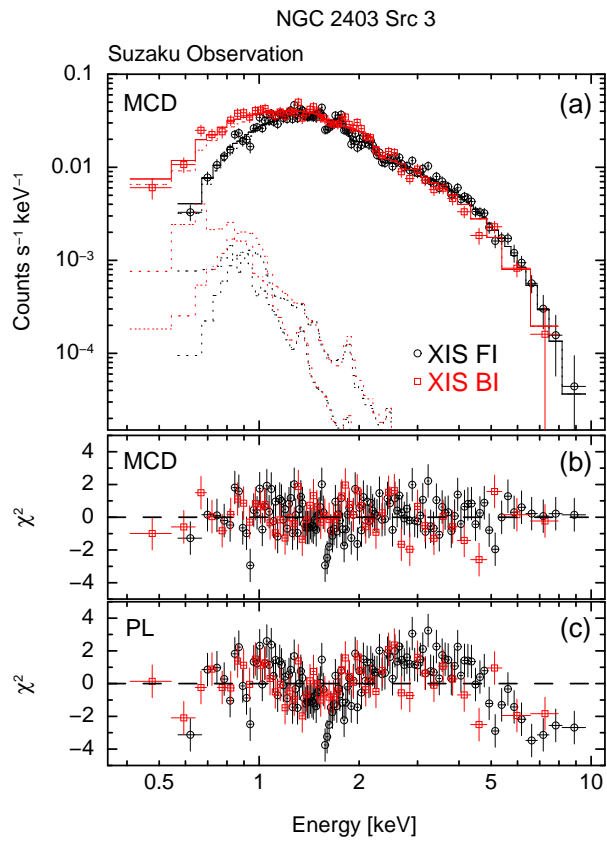


Fig. 3. (a) Suzaku XIS spectra of NGC 2403 Src 3, shown together with the best-fit MCD model. The FI and BI data are shown with black and red points, respectively. Two APEC components are also indicated (see text). The data are binned into pixels with at least 100 events. Panels (b) and (c) show the residuals from the MCD and PL models, respectively.

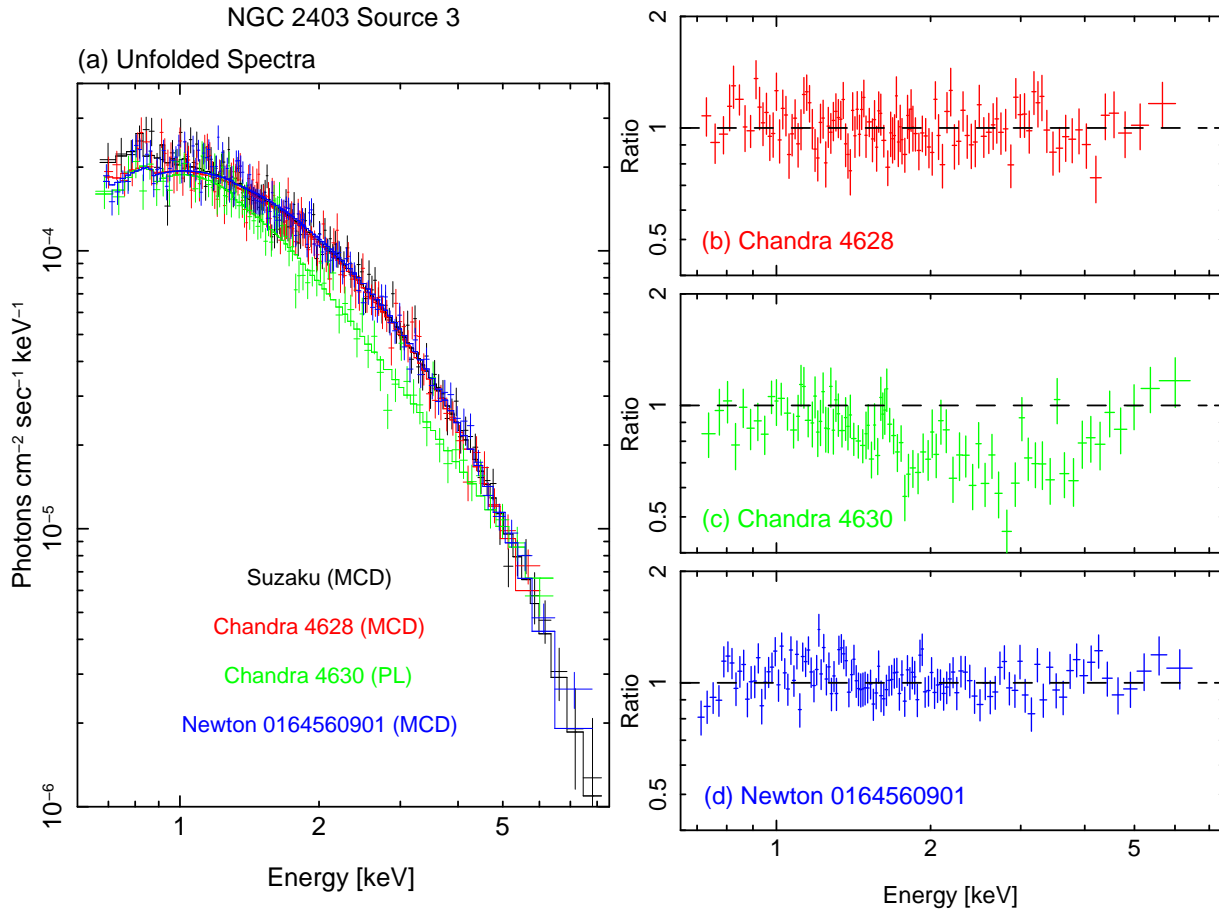


Fig. 4. (a) Unfolded spectra of NGC 2403 Src 3. The black, red, green and blue points indicate the Suzaku data, the Chandra data of ObsID = 4628, those of ObsID = 4630, and the XMM-Newton data of ObsID = 0164560901, respectively. Panels (b) - (d) show the Chandra and XMM-Newton spectra, divided by the prediction of the best-fit MCD model determined by the Suzaku spectrum. The color specification is the same as in panel (a)

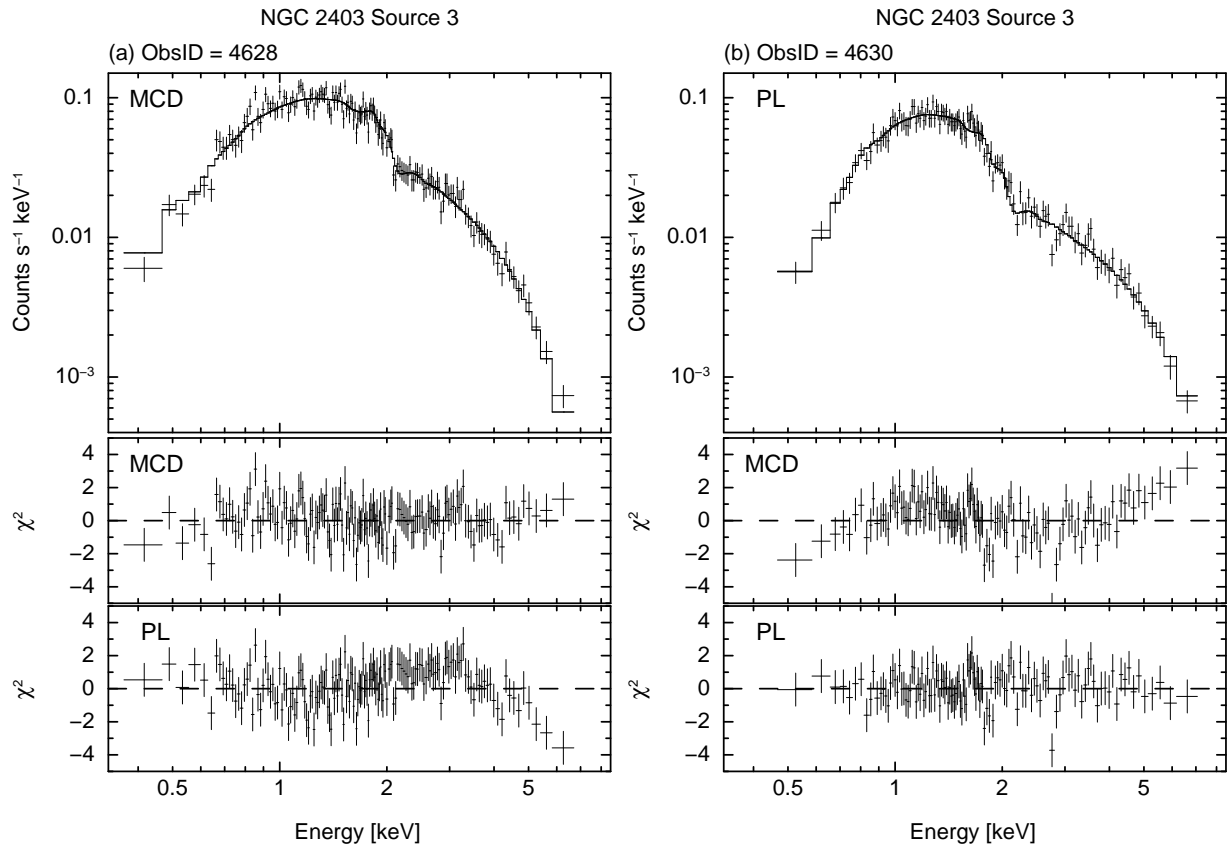


Fig. 5. Chandra ACIS spectra of NGC 2403 Src 3, from ObsID = 4628 (panel a) and ObsID = 4630 (panel b). The employed model is indicated in each panel.

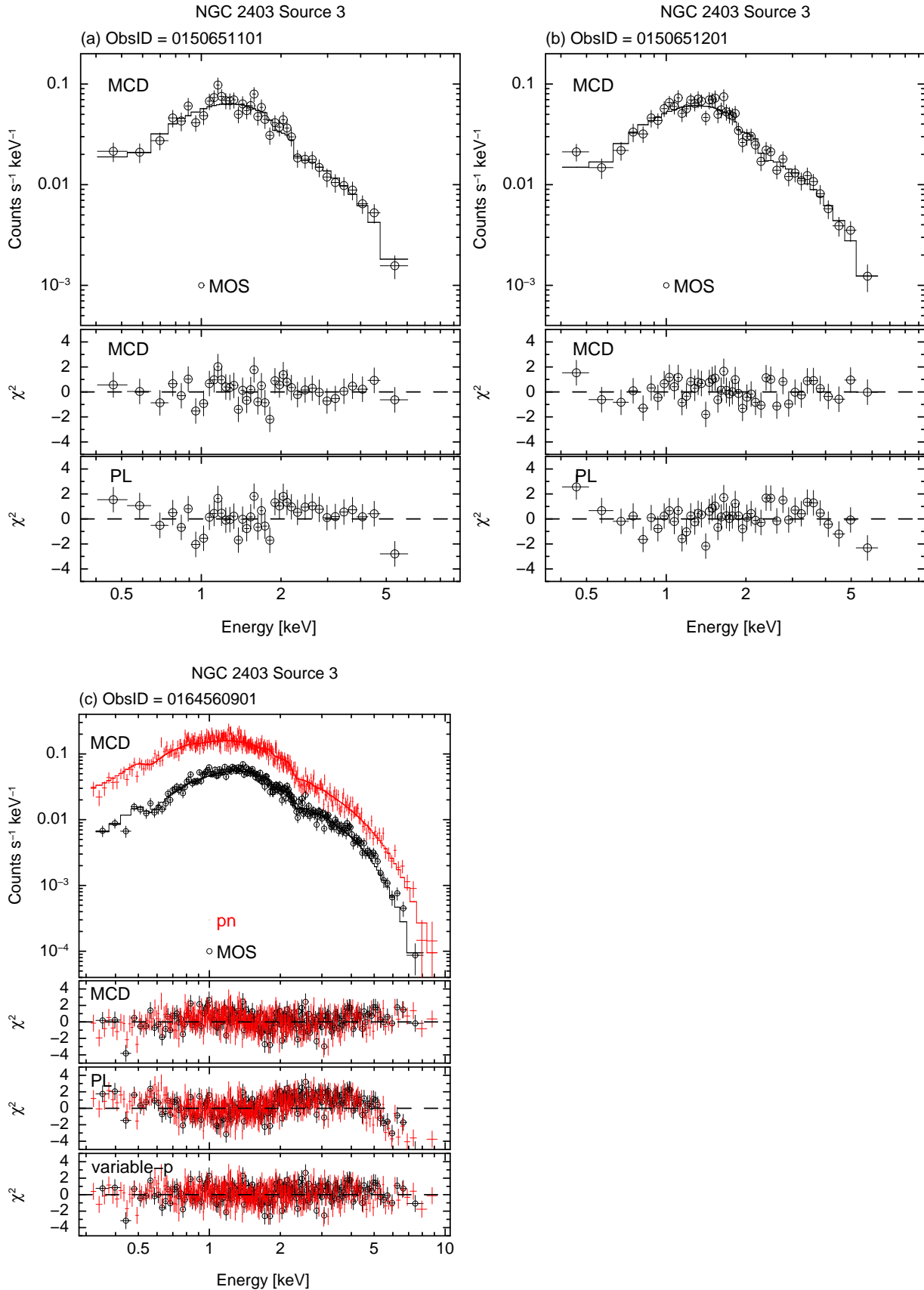


Fig. 6. XMM-Newton EPIC spectra of NGC 2403 Source 3, obtained on 3 occasions. The black, and red data points indicate the MOS and pn spectra, respectively. The histogram in the individual spectra indicate the best-fit MCD model. For the observation of ObsID = 0164560901 (panel c), the residuals of the variable-p disk model are also plotted.

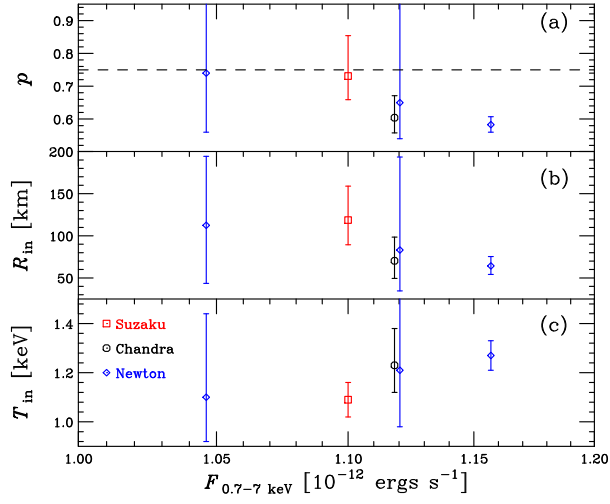


Fig. 7. A summary plot of the variable- p modeling of the Suzaku, Chandra, and XMM-Newton spectra of Src 3. Panels (a), (b) and (c) present p , R_{in} and T_{in} as a function of the observed 0.7 – 7 keV flux, respectively. The dotted line in panel (a) indicates $p = 0.75$.

A.0.1. X-ray spectra of NGC 2403 Src 5

The X-ray signals from NGC 2403 Src 5 is clearly detected in figure 1. We briefly analyze the X-ray spectrum of Src 5, although we regard that a detailed study of the source is beyond the scope of the present paper, due to relatively low signal statistics.

The X-ray signals from Src 5 and background are extracted from the circles denoted as **Src5** and **BGD5** in figure 1, respectively. Figure 8 shows the XIS spectra of Src 5. After calculating the rmf and arf files in the same way as for Src 3, the MCD and PL models were applied to the spectrum. We did not include the thermal components from the galaxy in the fitting, since the signal statistics are rather low and Src 5 is located slightly outside the diffuse emission (see figure 1). The absorption column density for the MCD model was fixed at the Galactic value, since it was unconstrained from the data.

The results of this analysis are summarised in table 6. Thus, the MCD model was moderately successful, and yielded the disk parameters as $T_{\text{in}} = 1.52_{-0.11}^{+0.13}$ keV and $R_{\text{in}} = 28.6_{-3.7}^{+4.1} \alpha^{1/2}$ km. The bolometric luminosity was estimated to be $L_{\text{bol}} = 4.0 \times 10^{38} \alpha$ ergs s⁻¹. The PL fit was slightly less successful, and gave a photon index of $\Gamma = 1.65_{-0.12}^{+0.13}$.

Table 6. Best-fit parameters for to Suzaku spectra of Src 5.

	MCD	PL
N_{H} (10^{21} cm ⁻²)	0.41 [†]	$1.19_{-0.61}^{+0.73}$
T_{in} (keV)	$1.52_{-0.11}^{+0.13}$	–
R_{in} (km)	$28.6_{-3.7}^{+4.1}$	–
Γ	–	$1.65_{-0.12}^{+0.13}$
L^*	4.0	4.7
$\chi^2/\text{d.o.f.}$	138.8/121	150.5/121

* L_{bol} for the MCD model, or absorption-corrected 0.5 – 10 keV luminosity for the PL ones, in 10^{38} ergs s⁻¹.

† fixed at the Galactic value.

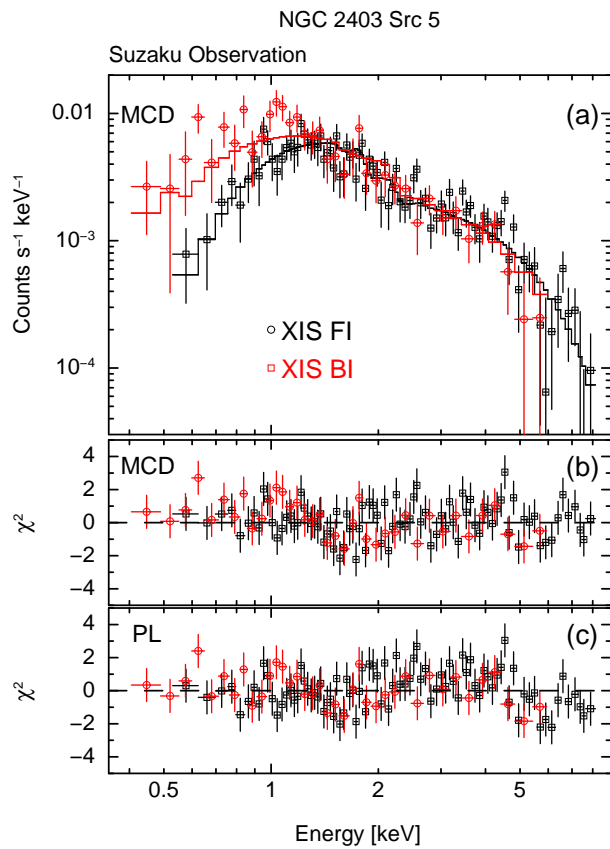


Fig. 8. Suzaku XIS spectra of NGC 2403 Src 5, shown in the same manner as figure 3.